Research Article | Vol. 29, No. 11 / 24 May 2021 / Optics Express 17011
Optics EXPRESS

Characterization of the optical encoder angular noise from terrestrial laser scanners

GAËL KERMARREC* AND JENS HARTMANN

Geodetic Institute, Leibniz Universität Hannover, Nienburger Str. 1, 30167 Hannover, Germany
*kermarrec@gih.uni-hannover.de

Abstract: Rigorous statistical testing of deformation using a terrestrial laser scanner (TLS) can avoid events such as structure collapses. Such a procedure necessitates an accurate description of the TLS measurements' noise, which should include the correlations between angles. Unfortunately, these correlations are often unaccounted for due to a lack of knowledge. This contribution addresses this challenge. We combine (i) a least-square approximation to extract the geometry of the TLS point cloud with the aim to analyze the residuals of the fitting and (ii) a specific filtering coupled with a maximum likelihood estimation to quantify the amount of flicker noise versus white noise. This allows us to set up fully populated variance covariance matrices of the TLS noise as a result.

1. Introduction

Terrestrial laser scanners (TLS) are contact-free measuring devices which can collect dense point clouds of many kinds of objects within a couple of minutes in situations where other topographical techniques reach their limits. After processing, coordinates are assigned to the recorded point. Each TLS system has its own characteristics, which determine the field and range of applications, i.e., the maximum range, resolution and accuracy of the distance measurement. Typical applications of TLS include industrial metrology, reverse engineering, cultural heritage, surveying, tunnel monitoring, forest canopy analysis, deformation monitoring, mobile mapping or quality assurance. The reader is referred to [1,2] and the references inside for a concise explanation of the TLS principles.

Basically, a TLS is a range finder: It measures a distance from a time difference [3]. In addition to the range, two polar angles, vertical and horizontal, are recorded to obtain a three-dimensional representation of the scene scanned. Two main approaches exist: (i) The time of flight, which enables two-target detection by "first-last pulse" evaluation and (ii) the phase approach, which uses the principle of radar technology transformed to laser wavelength modulation. Such scanners follow the amplitude and the optical frequency modulation of current waves technologies and are high precision TLS.

Unfortunately, the measurements of TLS are affected by both systematic and random errors. The former can be repeated in defined conditions and compensated for by calibrating (e.g., [4] and the references inside). On the contrary, random errors are not repeatable and cannot be removed as easily. They have to be estimated to improve the scanner's manufacturing and positional accuracy of point clouds; A realistic description of the variance and correlation of the noise measurements is mandatory to avoid biases in many geodetic quantities. Prominent applications are, for example, (i) the estimation of the parameter accuracy when the point clouds are approximated with parametric models, such as cylinders, planes or B-spline surfaces [5], or (ii) the definition of rigorous test statistics for deformation monitoring [6,7].

The range is the most important measurement of the TLS. The description of the random errors affecting this measurement has been the topic of various publications (e.g., [8] and the references inside for a point-wise variance model based on the intensity values recorded by a TLS). Further, the temporal correlations should not be neglected to avoid an overestimation of

#422735 https://doi.org/10.1364/OE.422735
Journal © 2021 Received 16 Feb 2021; revised 25 Mar 2021; accepted 28 Mar 2021; published 18 May 2021

Optics EXPRESS

the accuracy of the point clouds [9,10]. In addition to the range, a TLS measures two polar angles. The latter are often considered to be uncorrelated, i.e., the stochastic model is restricted to the description of the variances, which are taken from the manufacturer's datasheet. We are intended to think that the noise of the angle measurements will be highly correlated with time, particularly as the laser measuring frequency increases. Neglecting correlations is, thus, a strong simplification, made by lack of knowledge. This contribution deals to fill this gap by justifying, characterizing and calibrating the temporal correlations of the noise angle in order to set up an improved stochastic model for geodetic applications. To that aim, we will capture a plane with a TLS, as planes are simple objects often used to that intent. We will adjust the point clouds using a nonlinear least-square adjustment called the Gauss-Helmert model to filter the geometry of the point cloud with a high trustworthiness [11,12]. The residuals of the approximation are defined as the difference between the approximated and the original observations and depict the noise of the corresponding adjusted observations. We will propose a methodology to characterize the specific polar angle noise. We base our development on physical considerations concerning the correlation structure expected. Thus, an adequate filtering strategy combined with a maximum likelihood estimation (MLE) of the so-called Hurst exponent [13] is derived to estimate the ratio between white (WN) and correlated noise.

Our analysis provides a unique description of the encoder and oscillating mirror noise. The latter depends on the laser measurement frequency and gives a new insight into the performance of the scanner under consideration. Such information is never given by the manufacturer. The noise properties and particularly the temporal correlation of angles is, however, as important as the range: Their stochastic characteristics have to be calibrated to fill up a trustworthy variance covariance matrix of the raw TLS measurements [11]. The latter is mandatory for the aforementioned applications which necessitate an estimation of uncertainties.

The remainder of the paper is as follows: In a first section we will describe the different types of noises that are expected from oscillating mirrors and encoders and present our procedure to analyze the residuals of a plane adjustment based on the noise assumption. The following section presents the results of a real case experiment, which we conclude with some recommendations for statistical testing.

2. Methodology

In this section, we introduce the mathematical procedure used to derive the correlation structure of the TLS angle measurements, i.e., two polar angles. Accordingly, we briefly introduce the principle of the angle encoder and describe the noise structure that can be expected. We show how to use the residuals of a plane fitting from a TLS point cloud to investigate the amount of colored noise and WN.

2.1. TLS principle

2.1.1. Basic principles

The TLS are referred to as either terrestrial or topographic Light Detection And Ranging (LiDAR). They acquire numerous points by emitting laser pulses toward these points and measuring the distance from the device to the object [3]. A TLS scans its surrounding environment. It records measurements of a slant range using a laser range finder and two associated angles by angular encoders in the horizontal and vertical planes passing through the center of the instrument. Figure 1 shows the principle of rotating mirrors and the laser range finder. The deflection of the laser beam takes place in fixed angular increments, also called encoder steps, in horizontal and vertical directions; The environment is captured helix-wise. A typical commercial TLS scanner rotates 180° horizontally and 310° vertically, providing full coverage of an area in a short time frame. The angular resolution can be set by the user, although the same setting is usually chosen

Optics EXPRESS

for both directions. The distance measurements can be made either by pulse ranging, phase difference or a mixed form combining both methods–the description of these methods is not in the scope of this contribution and can be found in the dedicated literature mentioned previously. We will make use of a TLS based on phase shift measurement principle in this contribution.

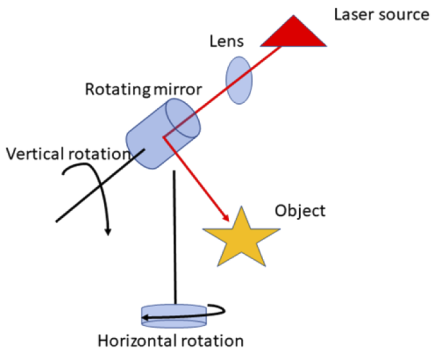

Fig. 1. Principle of the TLS angle measurements by means of rotating mirrors.

2.1.2. Angle encoder

Principle As depicted in Fig. 1, the deflections of the angles are realized by optical mirrors that either rotate or oscillate horizontally and vertically [14]. Angle encoders measure the rotational position and provide output that corresponds to the displacement by counting the number of rotations of the motor axis. As the motor rotates, the encoder relays the signal to the receiving device. This data only consists of either displacement pulses (incremental encoder) or initial and final absolute positions (absolute encoder, see [15,16] for a low-cost diffraction optical absolute encoder).

In this contribution, we made use of the Zoller + Fröhlich Imager 5016 (Zoller & Fröhlich GmbH, Wangen im Allgäu, Germany). The lines on the encoder disk of this instrument are optically scanned in two measuring channels offset by 90°. The cosine-shaped signals induced go between two adjacent encoder lines. As a result, angular positions between the encoder lines can be measured with a resolution of 0.00026° in the vertical and 0.00018° in the horizontal direction [17]. This interpolation takes place in the "encoder" itself, which outputs two–again 90° phase-shifted – A and B digital signals; Interpolating the signals of such a quadrature angle encoder increases its performance significantly. By treating the leading and trailing edge of both A and B signals as individual pulses, the effective resolution of the angle encoder is multiplied by a factor of 4. It should be noted, however, that errors or noise can be amplified through interpolation, i.e., the accuracy may not be enhanced with a higher resolution [18].

2.1.3. Encoder noise

Most of the encoders are susceptible to interference or electromechanical problems due to friction [19]. Although commercial encoders must be adapted to expensive anti-backlash gear-reduction systems, random measurement errors remain. In the following, we propose to briefly describe the type of noise expected from angular measurements.

White noise An encoder is an electromechanical device and its measurements are affected by noise. Different types of noise exist that are often classified or described by their "colour" from pink to red. They are related to the spectral slope of their power spectral density (psd), which refers to the spectral energy distribution that would be found per unit time [20]. In addition

Optics EXPRESS

to those noises, the thermal noise is common to nearly all electronic devices as it comes from the random thermal agitation of electrons in a conductor, which increases with frequency and temperature. It is a WN, i.e., a combination of a very large number of random events, and satisfies the conditions of Gaussian distribution [21].

Additionally, shot noise is caused by the random emission of individual electrons from a cathode [22] and often described in terms of a Poisson process [23]. It leads to a noise spectral density that is independent of frequency and can also be characterized as WN. Regarding encoders, this combination of WNs occurs during the transmission of the signal to the receiving electronics, especially when the cable lengths are long. False counts can occur that induce error in the position feedback.

Flicker noise Flicker noise (FN), also called 1/f noise, is a low-frequency electrical noise for which the noise power is inversely proportional to the frequency f [24]. It is a very sensitive measure of the quality and reliability of electrical components and electronic devices. Unfortunately, FN is present in all active and many passive devices and often considered to be related to imperfections in the crystalline structure of semiconductors [25]. It is associated with a direct current in electronic devices and increases as the frequency decreases, i.e., its spectral slope is in 1/f. The FN is, thus, an intermediate between the well understood WN with no correlation and the random walk (Brownian motion) noise with no correlation between the increments of the process under consideration. This noise has a widespread occurrence, although physical explanations for it are hard to find in the literature.

Combination of noise The total noise of the encoder is a combination of a FN and a broadband noise or WN coming from each component in the system, either passive or active. The typical psd of a noise combining FN and WN is shown in Fig. 2. The two noises are separated at a cutoff or corner frequency for which the psd of WN and FN are equal. Figure 2 (green line) shows the optimal case, where the corner frequency at −1.25 rad/sample in log plot is easily identifiable visually as the point where the WN slope of 0 breaks. It is depicted as the intersection between the blue and the red dotted line. As the amount of FN regarding the WN (Fig. 2 magenta line) increases, the psd has a more "global" slope but still allows for a visual identification of a corner frequency around −0.75 rad/sample.

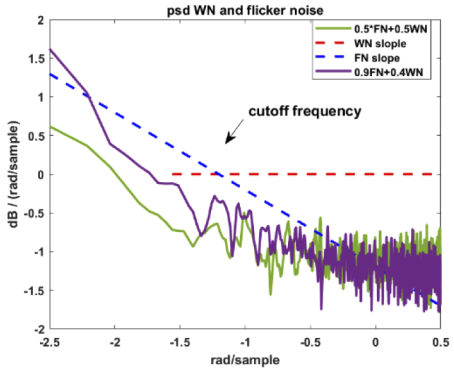

Fig. 2. The psd of the noise combination of the electronic device in log plot. The slopes of the psd for the WN (0) and the FN (−1) are given additionally in red and blue, respectively.

Optics EXPRESS

2.2. Least-squares as a filter: mathematical approximation of three-dimensional point clouds

We start from a raw point cloud of TLS observations scanned vertically "line-wise", corresponding to a plane which we extract from the point cloud in a preprocessing step. Figure 3 shows exemplarily 1500 epochs (1.5 scanning line) of the raw polar angles ϕ, λ using the resolutions extremelyhigh (EH) of a Zoller + Fröhlich Imager 5016 for a plane of 1×1 m, scanned at a distance of 5 m. As expected, the vertical angle ϕ increases linearly with time, whereas the horizontal component λ remains nearly constant until it is incremented after Δt; this value depends on the setting chosen for the measurements. The TLS is, thus, said to scan helix-wise.

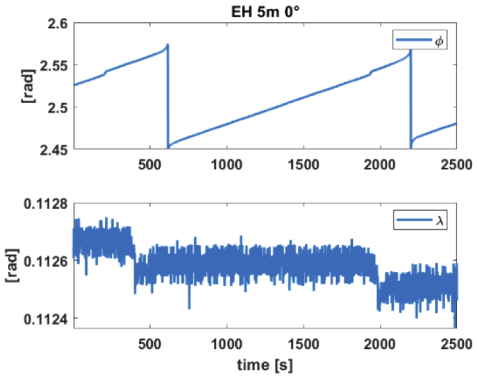

Fig. 3. Vertical and horizontal angles ϕ and λ, respectively, for the resolution extremely high (EH) for a plane (1×1 m) scanned at a distance of 5 m (no tilt).

We approximate the point cloud using a least-squares strategy. In the following, we propose describing the mathematical concept of the approximation briefly, focusing on how the residuals of the approximation can be used to derive the noise structure of the angle measurements.

2.2.1. Basic principles of plane fitting

A plane is an infinitively extended surface defined by a normal vector $\mathbf{n}^{\mathrm{T}} = \begin{pmatrix} n_x & n_y & n_z \end{pmatrix}$, with $\mathbf{n}^{\mathrm{T}}\mathbf{n} = 1$, and a distance parameter d, i.e.,

$$\mathbf{n}^{\mathrm{T}}\mathbf{P}_i = d, \tag{1}$$

where $\mathbf{P}_i$ is an arbitrary Cartesian point lying on the plane [26]. The raw polar observations of a TLS are transformed into their Cartesian representations by the transformation

$$\mathbf{P}_i = \begin{pmatrix} x \\ y \\ z \end{pmatrix}_i = \begin{pmatrix} r \sin\phi \cos\lambda \\ r \sin\phi \sin\lambda \\ r \cos\phi \end{pmatrix}_i. \tag{2}$$

We define $\hat{\mathbf{v}}_i^{\mathrm{T}} = \begin{pmatrix} \hat{v}_{x_i} & \hat{v}_{y_i} & \hat{v}_{z_i} \end{pmatrix}$ as the residuals of the approximation for point i, i.e., the component-wise difference between the adjusted and the observed Cartesian coordinates. We make the usual simplification that the stochasticity of the residuals mirrors the noise of the observations themselves–here, the Cartesian coordinates of the TLS points.

In this contribution, we wish to analyze the noise of the *polar* angles. The pointwise polar residuals for λ and ϕ are expressed by means of the coordinates and the Cartesian residuals of

Optics EXPRESS

point i recorded at time t_i, with $i = 1 \dots n$ and n the number of observations [26] as:

$$\begin{cases} \hat{v}_{\lambda_i} = \text{atan}\frac{y_i+\hat{v}_{y_i}}{x_i+\hat{v}_{x_i}} - \text{atan}\frac{y_i}{x_i} \\ \hat{v}_{\phi_i} = \text{atan}\frac{\sqrt{(x_i+\hat{v}_{x_i})^2+(y_i+\hat{v}_{y_i})^2}}{z_i+\hat{v}_{z_i}} - \text{atan}\frac{\sqrt{x_i^2+y_i^2}}{z_i}. \end{cases} \tag{3}$$

We further define $\hat{\mathbf{v}}_\phi(t) = [\hat{v}_{\phi_1}, \dots, \hat{v}_{\phi_n}]^T = [\hat{v}_\phi(t_1), \dots, \hat{v}_\phi(t_n)]^T$ and $\hat{\mathbf{v}}_\lambda(t) = [\hat{v}_{\lambda_1}, \dots, \hat{v}_{\lambda_n}]^T = [\hat{v}_\lambda(t_1), \dots, \hat{v}_\lambda(t_n)]^T$ as the polar angle residual vectors.

2.2.2. Residual analysis

To compute the residuals, the geometry of the point cloud has been eliminated; The least-squares approximation introduced in Section 2.2.1 can be understood as a filter of the underlying plane. Alternatives based on the same principle could be, e.g., underlying cylinders or ellipsoids. The residuals of the approximation after a backward transformation (Eq. (3)) correspond to the noise of the observations. The raw observations are recorded and sorted temporally, and so will the residuals be. In this contribution, we characterize the correlated angle noise from the residuals by means of two indicators:

- *Ratio $R_{FN/tot}$*

Following physical considerations, we assume that the coloured noise (COLO) will correspond to a FN, which will be confirmed by both visual inspection of the psd and MLE, see 2.2.3.

To compute $R_{FN/tot}$, we decompose the residuals into a WN and the coloured component as $\hat{\mathbf{v}}_\phi = \hat{\mathbf{v}}_{\phi,WN} + \hat{\mathbf{v}}_{\phi,FN}$, and $\hat{\mathbf{v}}_\lambda = \hat{\mathbf{v}}_{\lambda,WN} + \hat{\mathbf{v}}_{\lambda,FN}$, where $\hat{\mathbf{v}}_{WN}$ is the WN component, $\hat{\mathbf{v}}_{FN}$ the coloured (FN) component with variance σ^2_{FN} which can correspond to ϕ or λ, respectively. We call $\sigma^2_{\hat{v}\phi}$ and $\sigma^2_{\hat{v}\lambda}$ the variance of the corresponding residuals, simplified as $\sigma^2_{\hat{v}}$ in context. We define

$$R_{FN/tot} = 100 * \sigma^2_{FN}/\sigma^2_{\hat{v}}, \tag{4}$$

which is expressed in % for both angles with the corresponding subscript.

Note: A random walk component would manifest itself at low frequencies with less power than the FN and mainly comes from outliers and/or an inaccurate geometric object or functional model. Because we scan and adjust a plane, this additional noise should be accordingly reduced and is here not further considered.

- *the correlation coefficient r_c*

We define r_c as the correlation coefficient between the 0-mean weakly stationary residual vectors $\hat{\mathbf{v}}_\phi$ and $\hat{\mathbf{v}}_\lambda$. This coefficient represents a measure of similarity between the two angles noises. We compute r_c by fitting an autoregressive process of first order AR(1) to the covariance function $C(\tau) = C(\hat{v}_\varphi(t_i), \hat{v}_\lambda(t_i + \tau))$ with $i = 1 \dots n$ [27]. For each t_i, we have

$$C(\tau) = \sigma^2_{\varphi,\lambda}[1, r\_c, \dots, r\_c^n] \tag{5}$$

where $\sigma^2_{\varphi,\lambda}$ is defined as the covariance between the two residual vectors for a time lag $\tau = 0$. $r\_c \in [0, 1]$ gives an indication of the strength of the correlation between the angle noises; $r\_c = 0$ corresponds to the no-correlation case.

2.2.3. Filtering strategy to extract the FN

To compute $R_{FN/tot}$ from Eq. (4) and characterize the noise coming from the encoders and rotating mirrors, we need to filter the WN component from the FN. In this section, we propose to address the challenge of estimating the spectral exponent from a coloured noise corrupted by WN. To that aim, we will make use of the Butterworth filter of the first order, following [28].

Optics EXPRESS

Butterworth filter Butterworth filters are called maximally flat filters because, for a given order, they have the sharpest roll-off possible without inducing peaking in the Bode plot. The Butterworth filter changes from passband to stopband by achieving passband flatness, which is done at the expense of wide transition bands [29]. Thus, when using a Butterworth filter of first order as a low pass filter on the residuals, there is no sharp elimination of a band of high frequencies, which results in a smooth transition, without any lack of power at high frequencies. This is an important property when COLO is further analyzed to determine its spectral slope α: Estimators may provide a biased slope in the presence of missing frequency bands. Because we conjecture that $\alpha \approx 1$, which corresponds to a FN, we adapt the cutoff frequency of the Butterworth filter iteratively so that the filtered counterpart $\hat{\mathbf{v}}_{COLO}$ for ϕ and λ corresponds to a FN. With this methodology, we ensure that a FN and a WN are separated.

Whittle estimators of the spectral slope Our filtering proposal relies on the estimation of the spectral slope. Most of the spectral slope estimators determine the so-called Hurst exponent (see e.g., [12] for a short review of different methods). The Hurst exponent is related to the spectral slope of the psd by $H = (\alpha + 1)/2$ for a stationary fractional Gaussian noise [30]. Correspondingly, we have $H \approx 1$ for a FN. In this contribution, we will make use of the Whittle MLE to estimate H. This choice is justified by the search for a noise with a known Hurst exponent. The MLE performs poorly if the assumption of strict long-range dependence is incorrect or for short samples [31] but still performs well in the presence of a sinusoidal or polynomial pattern (Table 1 in [32]). Exact maximum likelihood inference can be performed for Gaussian data by evaluating the log-likelihood [33,34]. This procedure necessitates matrix inversions. These latter can be avoided using the Whittle estimator, which aims to provide faster estimation with only a slight inaccuracy. This estimator is unbiased, asymptotically efficient and permits one to obtain the Hurst parameter with a high trustworthiness for our specific application. Its derivation is given in [31].

We note that our methodology is made possible by the evidence of a two-slopes noise, which will be highlighted in the next section. Information criterion can be computed to compare between noise models to justify that the COLO is corresponding to a power law noise [35]. In this contribution, the easiness of the noise identification from the psd makes this additional step unnecessary.

2.2.4. Summary of the methodology

Figure 4 summarizes the methodology used in this contribution:

- Perform a plane fitting using a Gauss-Helmert model. An approximation with B-splines surface can be alternatively used in a more general case [10];
- Backward transform the residuals in polar coordinates;
- Separate the COLO and WN using a Butterworth filter of the first order by iterative computation of the cutoff frequency. The filtered COLO noise should correspond to a FN; we make use of a MLE to compute the Hurst exponent, which should be close to 1.

Optics EXPRESS

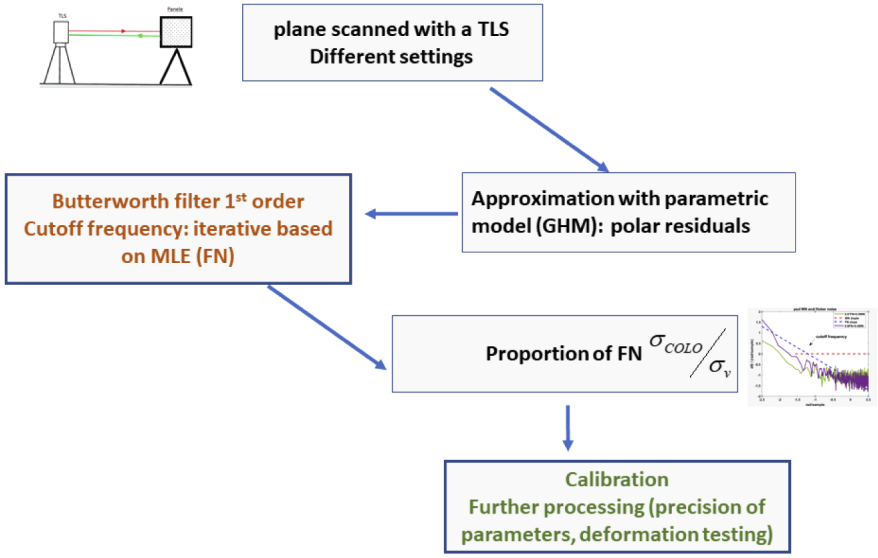

Fig. 4. Methodology to analyze the colored component noise from TLS angle measurements from the least-squares residuals.

3. Experiment and results

3.1. Description of the experiment

The analysis of the correlation structure of the angle measurements was performed by scanning a planar ALUCORE panel with a size of 1 × 1 m and a color of 43% white. We controlled the repeatability of the experiment by scanning the panel at two distances 2 and 5 m with a Zoller + Fröhlich Imager 5016. The measurements took place at the measuring laboratory of the Geodetic Institute, Leibniz University, Hannover, under stable conditions to avoid temperature variations. A reference scanning configuration was chosen. The laser scanner was set up at the height of the panel and with no tilting.

We eliminate points obviously not lying on the panel due to strong reflections and a resulting overexposure in the middle of the object using the least median of squared residuals, introduced by [36]. The data acquisition was performed with the resolutions "extremelyhigh" (EH), "ultrahigh" (UH), "superhigh" (SH) and "high" (H). The quality was set as "high." This resulted in a vertical rotation speed of 14 rounds per second. The corresponding laser measuring frequencies are given in Table 1.

Table 1. Laser measuring frequency [Hz] for different resolution settings for a Zoller + Fröhlich Imager 5016, quality high.

Resolution	Laser measuring frequency [Hz]	Time difference between measurements [s]
High H	136719	7.3E-06
Superhigh SH	273438	3.7E-06
Ultrahigh UH	546876	1.8E-06
Extremelyhigh EH	**1093752**	**9.1E-07**

Optics EXPRESS

3.2. Residual analysis

3.2.1. Processing

Following the methodology presented in Section 2.2, we analyze the polar angles noise from the residuals of the plane approximation combining an iterative filtering strategy to extract the WN with a MLE for the determination of the spectral slope of the FN. Our investigations should allow:

- For each polar angle, the quantification of the amount of FN depending on the settings used following Table 1 as well as the correlation r_c between the 2 angles,
- the analysis of the corner frequency of the Butterworth filter and its dependencies.

We performed the estimation of the indicators defined in Section 2.2.2 for one scanning line and took the mean over all scanning lines for the whole point cloud. This methodology reduces the impact of the outlier detection strategy by averaging the quantities as well as the impact of the small size of the plane scanned. This latter effect may lead to an unfavorable heteroscedasticity, i.e., a non-stationary variance, and a periodic pattern if more than one scanning line is considered for the estimation. The consequence would be the introduction of an unwanted random walk which would mislead the MLE and necessitate a specific low-frequency filtering.

The minimum batch size under the optimal scanning configuration (no tilt) for a panel scanned at 5 m distance was reached for the H resolution with 500 observations. The maximum batch size is 3000 observations for the EH setting at 2 m distance. The corresponding results are presented in Table 2 for the different settings. For the sake of brevity, we only present the results corresponding to the distance 5 m: The distance 2 m led to nearly the same results in a range of 1–2%. Additionally, we plot the psd of the residuals for the different case under consideration in Fig. 5 (left) in a log plot.

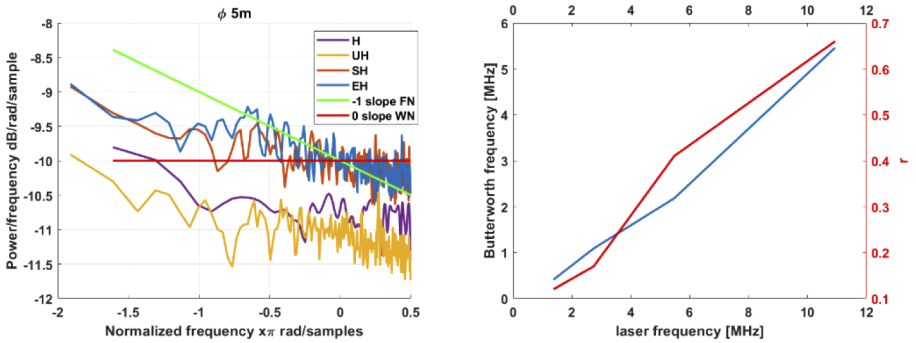

Fig. 5. (Left) psd of the residuals for the case 5 m (log plot). (Right) Butterworth cutoff frequency in MHz versus the laser measuring frequency (black axis) and correlation coefficient r_c between ϕ and λ noise (red axis).

Table 2. $R_{FN/tot}$ in % using different resolutions.

5 m [0.0]°	EH	UH	SH	H
ϕ	70%, 5.46 MHz	58%, 2.18 MHz	56%, 1.09 MHz	42%, 0.41 MHz
λ	66%, 5.46 MHz	51%, 2.18 MHz	56%, 1.09 MHz	40%, 0.41 MHz
r_c	**0.66**	**0.41**	**0.17**	**0.12**

3.2.2. Results of the analysis

The following conclusions can be drawn from Table 2 and Fig. 5:

Optics EXPRESS

- Figure 5 (left) highlights the two-slopes noise expected, i.e., a combination of FN (slope −1 at low frequencies, green line) and WN (slope 0 at high frequencies, red line). The cutoff frequencies can hardly be identified visually: This gives weight to the necessity of using a reliable estimator, such as the Whittle MLE, combined with a filtering with a Butterworth filter to extract the two noise components. We note the presence of specific frequencies in the high-frequency domain, which should correspond to the properties of the TLS under consideration. Their study is beyond the scope of this contribution.
- The ratio $R_{FN/tot}$ decreases with the laser measuring frequency (Fig. 5 right, black axis). As expected, it is higher (70%) for the setting EH, for which the mirror rotates at a higher speed rate. It decreases to 40% for the setting H. Similar results were found by scanning the object with a small tilt angle of 20°; the results are, thus, repeatable and a characteristic of the noise of the TLS under consideration.
- The ratio $R_{FN/tot}$ is nearly equal for the two angles, although slightly lower for λ . This finding highlights that the cause of the noise should be similar, i.e., coming from the oscillating mirror and the encoders' properties and not from the least-squares approximation or backward transformation.
- The correlation r_c between the noises from the two angle measurements depends linearly on the laser measuring frequency, as shown in Fig. 5 (right, red axis). The value found for the setting EH reaches 0.7, which is non-negligible for a correct modelling of the stochastic properties of the angle noise. However, we note that $\sigma^2_{\varphi,\lambda}$ was found 10 times lower than $\sigma^2_{v\varphi}$ and $\sigma^2_{v\lambda}$.
- Figure 5 (right, black axis) highlights the linear dependency of the Butterworth cutoff frequency on the laser measuring frequency. This finding is expected as the amount of WN increases as the measuring frequency decreases, i.e., for the setting H (Table 2, ratio around 40%). This linear dependency allows for a fully characterization of the angle noise, independently of the setting chosen.

3.3. *Application: improving the stochastic model for the TLS angle measurement*

In this section, we propose to show how the previous information can be used to build a realistic variance covariance matrix (VCM) for the TLS angle measurements. Such fully populated matrix can be used:

- in a least-squares adjustment for a trustworthy parameter estimation,
- for rigorous test statistic to avoid a potential detection of deformation that is due to the correlated noise and not to a real movement.

The VCM $\mathbf{\Sigma}_\phi, \mathbf{\Sigma}_\lambda$ corresponding to the two polar angles are symmetric positive definite matrices. Their diagonals contain the variances of the measurements, which can be either estimated from the residuals or taken from the manufacturer datasheet. The cross-diagonal elements are corresponding to the covariance between the observations. The fully populated VCM for the angle reads correspondingly:

$$\mathbf{\Sigma}_{angle} = \begin{bmatrix} \mathbf{\Sigma}_\phi & \mathbf{\Sigma}_{\phi,\lambda} \\ \mathbf{\Sigma}_{\phi,\lambda} & \mathbf{\Sigma}_\lambda \end{bmatrix}. \tag{6}$$

$\mathbf{\Sigma}_{\phi,\lambda}$ is filled using Eq. (5). $\mathbf{\Sigma}_\phi$ and $\mathbf{\Sigma}_\lambda$ are the VCM of the weakly stationary noise residuals ϕ and λ. One line of the matrix is given from [27] by

$$C(\tau) = \sigma^2_{\hat{v}} \left[\frac{R_{FN/tot}}{100} \frac{1}{2} (|\tau+1|^2 - 2|\tau|^2 + |\tau-1|^2) + \left(1 - \frac{R_{FN/tot}}{100}\right) \right] \tag{7}$$

Optics EXPRESS

which has to be adapted for ϕ and λ in context. The covariance function corresponds to a combination of FN and WN with τ being the time increment. It differs for ϕ and λ, as $R_{FN/tot}$.

Following the proposal of [27], a VCM for the range can be set up, leading to a point-wise fully populated VCM for the polar measurements $\mathbf{\Sigma}_{r,\phi,\lambda}$.

In its general form, the objective function of the least-squares adjustment to be minimized is given by $\mathbf{\Omega}(\mathbf{v}) = \mathbf{v}^{\mathrm{T}}\mathbf{\Sigma}^{-1}_{r,\phi,\lambda}\mathbf{v} = \min$ so that the prior knowledge of $\mathbf{\Sigma}_{r,\phi,\lambda}$ allows a trustworthy parameter estimation. When testing for deformation, we define the null hypothesis H_0 (no deformation occurs) and the alternative hypothesis H_1 as $H_0 : E\{\mathbf{\Delta}\} = 0$ versus $H_1 : E\{\mathbf{\Delta}\} \neq 0$, with $\mathbf{\Delta}$ the true difference between the two surfaces to be compared [37]. If we call $\hat{\mathbf{\Delta}}$ the difference computed from the estimated surfaces at the two epochs, a rigorous test statistics can be defined as $\mathrm{T}_{apriori} = \hat{\mathbf{\Delta}}^{\mathbf{T}}\mathbf{\Sigma}^{-1}_{\hat{\mathbf{\Delta}}\hat{\mathbf{\Delta}}}\hat{\mathbf{\Delta}}$, where $\mathbf{\Sigma}^{-1}_{\hat{\mathbf{\Delta}}\hat{\mathbf{\Delta}}}$ is the inverse of the VCM of $\hat{\mathbf{\Delta}}$. Without going into detailed derivations, the reader should intuitively understand that $\mathbf{\Sigma}^{-1}_{\hat{\mathbf{\Delta}}\hat{\mathbf{\Delta}}}$ depends on the $\mathbf{\Sigma}_{r,\phi,\lambda}$ of both point clouds and, thus, on the accurate description of the stochasticity of the polar measurements. The test decision relies on the quantile $k^{\chi^2_u}_{1-\alpha}$ which is based on the χ^2_u test distribution with u the degrees of freedom (number of observations minus number of estimated parameters) and α the significance level, typically 0.05. Exemplarily, H_0 is accepted if $\mathrm{T}_{apriori} \leq k^{\chi^2_u}_{1-\alpha}$.

4. Conclusions

In this contribution, we developed a method based on the approximation of TLS point clouds with least-squares combined with a filtering of its residuals with a Butterworth filter. The psd slope of the residuals was estimated with a Whittle MLE. This procedure was applied to analyze the noise structure of TLS angle measurements in order to derive (i) the amount of WN that can be expected regarding correlated noise and (ii) the correlation type of the angle noise, i.e., an expected FN.

In a controlled experiment, we made use of a 43% white panel scanned at 5 m under an optimal scanning configuration. The residuals of the approximation were analyzed based on the proposed methodology. The expected structure of the encoder and oscillating mirror noises were confirmed as being a combination of WN and FN, which could be calibrated. The Butterworth cutoff frequency for an optimal separation of the two noise sources was found to depend on the laser measuring frequency, thus allowing for a full characterization of the correlated noise. The correlation between the two angles highlighted the same linear relationship. These results can be used to derive a fully populated VCM for a more realistic description of the stochastic properties of the TLS angle noise. This latter can be used to avoid an overestimation of the precision from least-squares adjustment or test statistics, as used in deformation mqonitoring. Our finding highlighted that increasing the resolution by interpolation through quadrature angle encoders, as in the Zoller + Fröhlich Imager 5016, may not be linked to a better accuracy as the amount of FN increases accordingly. Further analysis will be performed with other TLS to compare the noise structure depending on the processing (time of flight, phase).

Funding. Deutsche Forschungsgemeinschaft (KE2453/2-1); Gottfried Wilhelm Leibniz Universität Hannover (Open Access fund).

Acknowledgments. The authors warmly thank Kamiel-Karl Heidberg for having performed the measurements. The publication of this article was funded by the Open Access fund of Leibniz Universität Hannover.

Disclosures. The authors declare no conflicts of interest

Data availability. Data underlying the results presented in this paper are available on demand

References

1. N. Pfeifer and C. Briese, "Laser scanning–principles and applications," *GeoSiberia 2007–International Exhibition and Scientific Congress. European Association of Geoscientists & Engineers* (2007).

Optics EXPRESS

2. S. Soudarissanane, R. Lindenbergh, M. Menenti, and P. Teunissen, "Scanning geometry: Influencing factor on the quality of terrestrial laser scanning points," ISPRS J. Photogramm. Remote Sens. **66**(4), 389–399 (2011).
3. G. Vosselman and H-G. Maas, eds., *Airborne and Terrestrial Laser Scanning* (Whittles, 2010).
4. D. D. Lichti and S. Jamtsho, "Angular resolution of terrestrial laser scanners," Photogramm. Rec. **21**(114), 141–160 (2006).
5. K. R. Koch, "Nurbs surface with changing shape," Allg. Vermess. Nachr. **3**, 83–89 (2010).
6. G. Kermarrec, B. Kargoll, and H. Alkhatib, "On the impact of correlations on the congruence test: A bootstrap approach," Acta Geod. Geophys. **55**(3), 495–513 (2020).
7. H. Pelzer, "Zur Analyse geodätischer Deformationsmessungen," Dtsch. Geodät. Komm. Ser. C. 164 (1971).
8. D. Wujanz, M. Burger, M. Mettenleiter, and F. Neitzel, "An intensity-based stochastic model for terrestrial laser scanners," ISPRS J. Photogramm. Remote Sens. **125**, 146–155 (2017).
9. C. Holst and H. Kuhlmann, "Challenges and present fields of action at laser scanner based deformation analyses," J. Appl. Geodesy **10**(1), 17–25 (2016).
10. G. Kermarrec, B. Kargoll, and H. Alkhatib, "Deformation analysis using B-spline surface with correlated terrestrial laser scanner observations – a bridge under load," Remote Sens. **12**(5), 829 (2020).
11. K. R. Koch, *Parameter Estimation and Hypothesis Testing in Linear Models* (Springer International Publishing, 1999).
12. J-M. Bardet, G. Lang, G. Oppenheim, A. Philippe, S. Stoev, and M. S. Taqqu, "Semi-parametric estimation of the long-range dependence parameter: A survey," in *Theory and Applications of Long-range Dependence* (Birkhäuser, 2003), pp. 557–577.
13. F. Neitzel, "Generalization of total least-squares on example of unweighted and weighted 2D similarity transformation," J. Geod. **84**(12), 751–762 (2010).
14. Y. Reshetyuk, *Investigation and Calibration of Pulsed Time-of-flight Terrestrial Laser Scanners*, (Trita-TEC-LIC, 2006).
15. S. Alvarez-Rodríguez and N. Alcalá-Ochoa, "Low-cost encoder using a phase shifting algorithm utilizing polarization properties of light," Appl. Opt. **55**(33), 9450–9458 (2016).
16. S. Alvarez-Rodríguez, F. G. Gerardo Peña-Lecona, M. Briones, M. Helguera, and N. Alcalá-Ochoa, "Low-cost non-concentric diffraction-based encoder," Opt. Laser Technol. **138**, 106836 (2021).
17. . Zoller + Fröhlich GmbH, "Z + F IMAGER 5016, 3d laser scanner data sheet" (2017), https://www.zf-laser.com/Z-F-IMAGER-R-5016.184.0.html.
18. H. Austerlitz, "Analog signal transducers," In *Data Acquisition Techniques Using PCs*, 2nd ed. (Academic Press, 2003), pp. 6–28.
19. S. Alvarez-Rodrígue, N. Alcalá-Ochoa, J. Cruz-Salgado, and F. G. Peña Lecona, "Suppression of noise to obtain a high-performance low-cost optical encoder," J. Sens. **2018**, 1–10 (2018).
20. L. Ward and P. Greenwood, "1/f noise," Scholarpedia **2**(12), 1537 (2007).
21. F. F. Mazda, *Telecommunications Engineer's Reference Book* (Butterworth-Heinemann, 1993).
22. B. Levush, K. L. Jensen, and Y. Y. Lau, "A comparison of flicker noise and shot noise on a hot cathode," IEEE Trans. Plasma Sci. **28**(3), 794–797 (2000).
23. G. A. Mihram, *Simulation. Statistical Foundations and Methodology. Mathematics in Science and Engineering*. (Academic Press, 1972).
24. F. N. Hooge, "1/f noise sources," IEEE Trans. Electron Devices **41**(11), 1926–1935 (1994).
25. B. Carter, "Op amp noise theory and applications," in *Op Amps for Everyone*, 3rd ed. (Newnes/Elsevier, 2009), pp. 163–188.
26. I. N. Bronshtein, H. Muehlig, G. Musiol, and K. A. Semendiaev, *Handbook of Mathematics*, 5th ed. (Springer, 2007).
27. G. Kermarrec, M. Lösler, and J. Hartmann, "Analysis of the temporal correlations of TLS range observations from plane fitting residuals," ISPRS J. Photogramm. Remote Sens. **171**, 119–132 (2021).
28. G. Kermarrec, "On estimating the Hurst parameter from least-squares residuals. Case study: Correlated terrestrial laser scanner range noise," Mathematics **8**(5), 674 (2020).
29. S. Butterworth, "On the theory of filter amplifiers," Wireless Eng. **7**, 536–541 (1930).
30. B. B. Mandelbrot, *The Fractional Geometry of Nature* (Birkhäuser, 1987).
31. A. M. Sykulski, S. C. Olhede, A. P. Guillaumin, J. M. Lilly, and J. J. Early, "The debiased Whittle likelihood," Biometrika **106**(2), 251–266 (2019).
32. P. Abry and D. Veitch, "Wavelet analysis of long-range-dependent traffic," IEEE Trans. Inform. Theory **44**(1), 2–15 (1998).
33. P. J. Brockwell and R. A. Davis, *Time Series: Theory and Methods*, (Springer, 1991).
34. P. Whittle, "Estimation and information in stationary time series," Ark. Mat. **2**(5), 423–434 (1953).
35. M. S. Bos, J.-P. Montillet, S. D. Williams, and R. M. Fernandes, "Introduction to geodetic time series analysis," arXiv: Other Statistics, 29–52 (2020).
36. P. J. Rousseeuw, "Least median of squares regression," J. Am. Stat. Assoc. **79**(388), 871–880 (1984).
37. W. F. Caspary, W. Haen, and H. Borutta, "Deformation Analysis by Statistical Methods," Technometrics **32**(1), 49–57 (1990).